

Dynamical thermalization and turbulence in social stratification models

Klaus M. Frahm¹ and Dima L. Shepelyansky^{1,2}

¹*Univ Toulouse, CNRS, Laboratoire de Physique Théorique, Toulouse, France*

²**Author to whom correspondence should be addressed: dima@irsamc.ups-tlse.fr**

(Dated: March 25, 2026)

We study the nonlinear chaotic dynamics in a system of linear oscillators coupled by social network links with an additional stratification of oscillator energies, or frequencies, and supplementary nonlinear interactions. It is argued that this system can be viewed as a model of social stratification in a society with nonlinear interacting agents with energies playing a role of wealth states of society. The Hamiltonian evolution is characterized by two integrals of motion being energy and probability norm. Above a certain chaos border the chaotic dynamics leads to dynamical thermalization with the Rayleigh-Jeans (RJ) distribution over states with given energy or wealth. At low energies, this distribution has RJ condensation of norm at low energy modes. We point out a similarity of this condensation with the wealth inequality in the world countries where about a half of population owns only a couple of percent of the total wealth. In the presence of energy pumping and absorption, the system reveals features of the Kolmogorov-Zakharov turbulence of nonlinear waves.

PACS numbers:

A mathematical model of social stratification in a society is introduced and investigated. The wealth levels of society are associated with energy levels of nearly constant density of states coupled by social network links between agents. It is shown that above a chaos border the nonlinear interactions between agents lead to chaos induced dynamical thermalization with the Rayleigh-Jeans (RJ) distribution over states. The distribution is characterized by temperature and chemical potential related to two integrals of nonlinear dynamics being system energy and the total probability norm. At low energy and temperature there is a phenomenon of RJ condensation actively studied experimentally and theoretically for light propagation in multimode optical fibers. Due to condensation a significant norm fraction is concentrated at lowest energy or wealth states. It is argued that such a RJ condensation describes the existence of a huge phase of poor households in a society and a tiny oligarchic phase that owns a big fraction of total wealth. In presence of energy injection at low energy states and absorption at high energies, a flow of energy or wealth from low to high energy modes appears which is similar to the Kolmogorov-Zakharov turbulence spectra of nonlinear waves. The Lorenz curves for wealth of households, obtained from the steady-state RJ distributions, are shown to be similar to the wealth distributions of households in the world countries.

I. INTRODUCTION

Social stratification is a society structure based on ranking of its members and groups being classified on the grounds of their wealth, activity, education and other re-

lated factors. This field is under active investigations in social and economy sciences starting from the theory of society class structure of Karl Marx (see e.g. [1–5]). Due to its complexity it can be useful to propose a mathematical model of social stratification of society (SSS) and study its properties with tools of dynamical nonlinear systems. One of the arguments for a construction of such SSS models is a recent enormous development of various social networks that gained a significant importance for communications, opinion formation and interactions between society agents (see e.g. [6, 7]). The properties of numerous social networks have been studied by various groups as reviewed in [6, 7]. However, all these studied are based on a linear matrix algebra of links between network nodes provided by their adjacency matrix of real systems. At the same time the interactions between society members are very complex and it is evident that they should include nonlinear interactions. Another feature, usually absent in studied social networks, is that commonly their adjacency matrix is composed only by off-diagonal links with zero diagonal component while it is natural to expect that social stratification should be related to the presence of a certain diagonal component attached to e.g. wealth inequality in a society.

In this work, we introduce a mathematical SSS model of interacting agents which has typical social network structure of links between agents but in addition also includes a nonlinear interaction of agents and social stratification described by a linear diagonal term added to an adjacency matrix. The proposed SSS model is associated to the following Hamiltonian:

$$\mathcal{H} = \sum_{n,n'} \psi_n^* H_{n,n'} \psi_{n'} + \frac{\beta}{2} \sum_n |\psi_n|^4. \quad (1)$$

which describes the dynamical evolution of a nonlinear field ψ_n for agents $1 \leq n \leq N$.

In fact, this is a classical Hamiltonian of an oscillator system if we present complex amplitudes of agent n as

$\psi_n = (q_n + ip_n)/\sqrt{2}$ with canonical coordinates q_n and p_n of coordinate and momentum. Then the time evolution of the system is given by

$$i\frac{\partial\psi_n(t)}{\partial t} = \sum_{n'=1}^N H_{n,n'}\psi_{n'}(t) + \beta|\psi_n(t)|^2\psi_n(t) \quad (2)$$

where the parameter β describes the strength of the nonlinear perturbation and $H_{n,n'}$ are the matrix elements of a real symmetric matrix H which will be specified more explicitly in the next Section. For $\beta = 0$, (2) represents a quantum Schrödinger equation or a simple coupled linear oscillator system where different oscillator modes are coupled by the matrix H .

The dynamical system (2) has two integrals of motion which are the quantity $\eta = \sum_n |\psi_n|^2$ (or weighted number of agents), called *norm* [49], and the *classical oscillator energy* \mathcal{H} in (1). Here, we fix the norm to $\eta = 1$. The case $\eta \neq 1$ can be reduced to the case $\eta = 1$ by a suitable rescaling of ψ and β .

In the SSS model, which will be defined more precisely in the next Section, the nonlinear fields ψ_n describe N society agents, nondiagonal elements $H_{n,n'}$ represent social network links between agents with nonlinear interactions induced by the β -term while the diagonal elements $H_{n,n}$ characterize social stratification.

According to the general properties of dynamical chaos [8–11], we expect that at a moderate value of the nonlinear parameter β above a certain chaos border β_{ch} , the dynamics becomes globally chaotic with positive maximal Lyapunov exponent and positive Kolmogorov-Sinai entropy. Below the chaos border the dynamics is integrable according to the Kolmogorov-Arnold-Moser (KAM) theorem [8–11]. The chaotic dynamics should lead to dynamical thermalization of the system to a state of maximal entropy on the phase space defined by the two integrals of motion.

This particular case leads to the Rayleigh-Jeans (RJ) thermal distribution over linear eigenmodes of the matrix H [12, 13]:

$$\rho_m = \frac{T}{E_m - \mu} \text{ (RJ)} \quad (3)$$

where ρ_m is the average occupation number of the oscillator mode at energy E_m ; T and μ are the temperature and chemical potential determined by the values of the two integrals of motion (see next Section for more technical details).

We stress that in our model the RJ thermalization has a purely dynamical origin due to the chaotic dynamics and that there is no contact with a thermal bath. The issue of dynamical thermalization in such oscillator chains (with nonlinear perturbations) has a long and complicated history with the first numerical experiments performed by Fermi-Pasta-Ulam-Tsingu (FPUT) on the MANIAC I computer in 1955 with the conclusion that “The results show very little, if any, tendency toward equipartition of energy between the degrees of freedom”

[14]. Later it was shown that the absence of thermalization in the FPUT model was due to small nonlinear values of couplings between oscillators and the system proximity to completely integrable nonlinear models e.g. like the Toda lattice. At a stronger nonlinearity, above the chaos border, the dynamical thermalization was recovered (see the extensive literature about the FPUT problem e.g. in [15–19] and Refs. therein). The FPUT model has only one integral of energy so that in the thermalized regime the average energy of each linear mode is equal to temperature T ($\mu = 0$ in (3)).

In [20], it was argued that the proximity to integrable models can be excluded for the case when the matrix H of linear couplings between harmonic oscillator modes, in Eqs. (1), (2), is random according to Random Matrix Theory (RMT) which describes the universal properties of spectra and eigenstates of complex nuclei, atoms and molecules [21, 22]. It was shown in [20] that for an RMT matrix H a moderate nonlinearity β above a certain chaos border chaos indeed leads to RJ thermalization with the distribution (3) both for positive and negative temperatures T .

The RJ thermalization has also been established for a more realistic model of light propagation in a quantum chaos fiber, described by a nonlinear Schrödinger equation (NSE), if the nonlinearity is sufficiently strong [23]. In such a fiber the NSE depicts the propagation along a fiber, with the longitudinal coordinate z corresponding to time, and the D-shape of the fiber cross-section leads to quantum chaos of linear eigenmodes creating RMT type properties of the matrix H in (1).

We point out that RJ thermalization has also been actively studied numerically and experimentally in the context of light propagation in multimode optical fibers [24–30]. At the same time the origins of this thermalization were attributed to the Kolmogorov-Zakharov (KZ) turbulence [13, 31, 31, 32] without referring to chaos and KAM integrability. At low temperatures the RJ distribution may have an enormous norm concentration at the ground state mode and the emergence of this *RJ condensation* was established numerically in [26] and experimentally in [25, 27].

We may also note that the Fröhlich condensate for biomolecules at room temperature, proposed in [33, 34], has certain similarities with the RJ condensate showing analytically that the RJ distribution (3) has a huge norm concentration at the lowest frequency mode even though in [33, 34] the considered system includes external pumping and dissipation (see also the discussion in [23]).

The RJ thermalization observed in [20] is due to the combination of the nonlinear term and the RMT structure of H which is very different from the link structure of social networks described by very sparse matrices with small-world properties [6, 7]. In [35], dynamical RJ thermalization was discussed for such a case where the matrix H is constructed from a real social network but due to the absence of diagonal terms (absence of self links) this model has no social stratification.

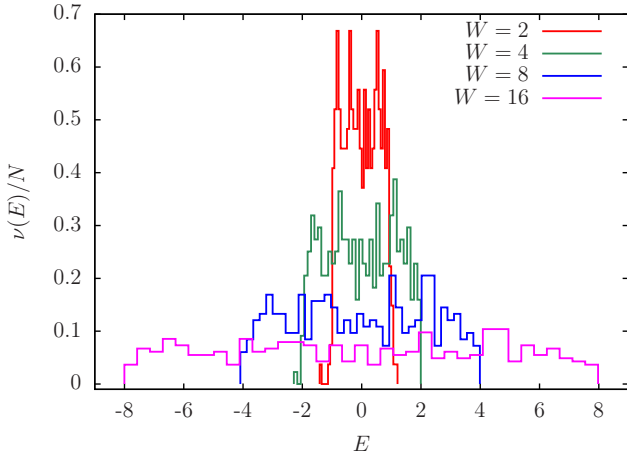


FIG. 1: Rescaled density of states $\nu(E)/N$ with $\nu(E) = dm/dE_m$ for the energy eigenvalues E_m of the matrix H for the SSS model at $W = 2, 4, 8, 16$ given by (8) for $f = 0.1$ and $\kappa = 0.5$. The normalization is given by $\int dE \nu(E) = N$.

In this work, we consider a more realistic SSS model with social network links and also with a social stratification modeled by additional diagonal matrix elements in H and where nonlinear interactions and dynamical chaos also lead to RJ thermalization and condensation for suitable choices of system parameters. Here the linear eigenenergies E_m have a rather constant density of states. For a society such energy levels E_m (or oscillator frequencies) can be considered as certain levels of wealth of society agents with low and high energies corresponding to poor and rich people in a human society. Then the RJ condensation at low energy states can be considered as a phase of poor population at low wealth while a population fraction at high energies (or wealth) can be viewed as an oligarchic phase of very rich people. We highlight a certain similarity between RJ condensation in these SSS models and the wealth inequality in the human society where for the whole world 50% of the population owns only 2% of total wealth, while 10% of population owns 75% of total wealth and 1% of population owns 38% of total wealth [36, 37].

We mainly focus on the SSS model with Hamiltonian dynamics according to (1), (2). However, following the approach of [38], we also consider a modified model with pumping (absorption) of energy and norm at low (high) energy eigenmodes. This creates a turbulent flow from low energy states (poor wealth layer of society) to high energy states (rich wealth society layers) which is in a sense similar to the KZ turbulent energy flow from long to short wave lengths [13]. We argue that this SSS turbulent system can be viewed as a simplified mathematical model of Marxist theory for classes and wealth distribution in a society.

The work is constructed as follows: the model description is given in Section II with some additional technical details about RJ thermalization, numerical method and studied quantities, results for chaotic Hamiltonian dy-

namics are presented in Section III, the results for the case with pumping and absorption corresponding to dynamical turbulence are given in Section IV, Lorenz curves of wealth inequality described by the considered models are presented in Section V and the discussion of the results is given in Section VI.

II. MODEL DESCRIPTION

A. RJ thermalization and Entropy

Assuming chaotic dynamics for a sufficiently large value of β , the Hamiltonian system (2) corresponds to the specific case of a microcanonical ensemble, with conserved energy $\mathcal{H} = E$ and with an additional constraint for the norm parameter $\eta = 1$ which is also conserved. Technically, it is more convenient to treat this ensemble in the framework of the grand canonical ensemble which is justified in the limit $N \gg 1$. Then the quantities η and \mathcal{H} may fluctuate “freely” and only their average values are fixed by $\langle \eta \rangle = 1$ and $\langle \mathcal{H} \rangle = E$ with some given energy E value which is a parameter of the model.

This particular case leads to the Rayleigh-Jeans (RJ) thermal distribution over linear eigenmodes $\phi_n^{(m)}$ of the matrix H with eigenenergies E_m (which are taken to be ordered $E_1 < E_2 < \dots < E_N$). Here it is assumed that the typical contribution of the β -term in (1) to the global energy is small which corresponds to $\xi \gg 1$ where $\xi = (\sum_n |\psi_n|^4)^{-1}$ is the inverse participation ratio (IPR) of the state in the initial basis. This assumption is typically well verified once we are in the thermalized regime. However, at initial times and depending on the initial condition it is possible that ξ is not very large which may lead to a rather significant shift of the *linear* energy contribution (first term in (1)) between the initial and the thermalized state. This point will be discussed later in more detail for some examples.

Using the eigenmodes $\phi_n^{(m)}$ of H , the wave function at time t can be presented as $\psi_n(t) = \sum_m C_m(t) \phi_n^{(m)}$ with mode amplitudes $C_m(t)$. Then the thermalized statistical RJ distribution of the complex eigenmode amplitudes C_m are independent (complex) Gaussian distributions with the theoretical average $\langle |C_m|^2 \rangle = \rho_m = T/(E_m - \mu)$ [12, 13] where the parameters T and μ are the system temperature and chemical potential determined by the average constraints:

$$E = \mathcal{H} \approx \sum_m E_m \rho_m \quad , \quad 1 = \langle \eta \rangle = \sum_m \rho_m \quad . \quad (4)$$

Both expressions (3) and (4) imply that $(E - \mu)/N = 1/N \sum_m (E_m - \mu) \rho_m = T$ which gives a direct implicit equation for $\mu(E)$ using the 2nd equation of (4)

$$1 = \frac{1}{N} \sum_m \frac{E - \mu}{E_m - \mu} \quad . \quad (5)$$

This equation provides one physically valid solution $\mu(E)$ with either $\mu < E_1$ (for $T > 0$) or $\mu > E_N$ (for $T < 0$) such that $\rho_m > 0$ is well verified for all modes [50]. Once $\mu(E)$ is known (from a numerical solution of (5)), one immediately obtains $T(E) = (E - \mu(E))/N$.

We mention that the RJ distribution is a limiting case of the Bose-Einstein distribution, for quantum oscillators, at high temperatures $T \gg E_m - \mu$:

$$\rho_m = \frac{1}{\exp[(E_m - \mu)/T] - 1} \quad (\text{BE}). \quad (6)$$

The steady-state RJ distribution of ρ_m (3) allows also to determine the von Neumann entropy S_q , analogous to the quantum entropy, and the classical Boltzmann entropy S_B given by the expressions [23, 24]:

$$S_q = - \sum_m \rho_m \ln \rho_m, \quad S_B = \sum_m \ln(\rho_m) + S_0 \quad (7)$$

where S_0 is a constant which we choose arbitrarily as $S_0 = N[1 + \ln(N^2\pi)]$ to fix a certain numerical offset which ensures that typically $S_B > 0$ and that S_B/N and S_q have comparable values. (See also [35] for a motivation of this choice using elementary phase space cells of volume h_B^N with $h_B = 1/N^2$.) We mention, that the expression for S_B is initially derived for the case of the thermalized situation but it can be quite easily verified [35] that this expression is also valid outside equilibrium if we assume that the amplitudes C_m have still independent Gaussian distributions but with arbitrary averages $\langle |C_m|^2 \rangle = \rho_m$ where ρ_m are arbitrary parameters which are potentially different from their thermalized values (3). This point is important when using (7) for numerically data at shorter time values outside equilibrium. For the Boltzmann entropy we have the usual thermodynamic relation $dS_B/dE = 1/T$ [12, 23, 24, 35] while the von Neumann entropy S_q determines effectively a populated number of states at system energy E . We mention that the relation $dS_B/dE = 1/T$ can also be verified directly by a simple calculation from (7) using the thermalized expressions $\rho_m(E) = T/(E_m - \mu(E))$, $T(E) = (E - \mu(E))/N$ since the condition $\sum_m \rho_m = 1$ ensures that the contributions $\sim \mu'(E)$ drop out. Certain properties of S_q and S_B are also discussed in [23, 35].

B. Hamiltonian dynamics in the SSS models

To model the social network links of a weighted adjacency matrix A_{ij} , we choose the real network of scientific collaboration collected by Mark Newman [39–42] with values of A_{ij} given by Eq. (2) of [40] and which are taken directly from the raw data of [40, 41]. This nondirected network with $A_{ij} = A_{ji}$ has $N = 379$ nodes and $N_\ell = 1828$ off-diagonal links with a moderate average number of links per node $\chi \approx 4.82$ (all other matrix elements of A_{ij} are zero). Therefore the matrix A is very sparse. Links $i \rightarrow j$ and $j \rightarrow i$ for different nodes $j \neq i$

are counted twice in the definition of N_ℓ and self links $i \rightarrow i$ are absent.

In the following, we choose the matrix H in (2) as

$$H = D + f(A + \kappa H^{\text{GOE}}) \quad (8)$$

where A is the adjacency matrix introduced above using the data of [40], D is a diagonal matrix (see below for details) and H^{GOE} is a random GOE-matrix [21, 22], with a semicircle density of states of radius unity (at large $N \gg 1$), which has random Gaussian matrix elements with zero mean and variance $\langle (H_{n,n'}^{\text{GOE}})^2 \rangle = (1 + \delta_{n,n'})/(4(N+1))$. Furthermore, the parameter $f = 0.1$ is a simple scaling factor and $\kappa = 0.5$ is a coefficient for the weight of H^{GOE} .

The matrix H^{GOE} is introduced to remove a significant number of degeneracies in the eigenvalue spectrum of the adjacency matrix A (which typically has simple fractions for the non-zero matrix elements and a quite particular algebraic structure). At $\kappa = 0.5$, the effect of the degeneracies for the eigenvalues of $A + \kappa H^{\text{GOE}}$ are “smoothed out” while the global form of the density of states is not significantly modified which is illustrated in Fig. II.1 of [35]. Furthermore, in [35], further details on the degeneracies of A and its particular eigenmode structure are discussed.

The case $D = 0$, $f = 1$ has been discussed in detail in [35] concerning the properties of H and the issue of RJ thermalization in (2). In particular, Fig. II.1 of [35] shows that the eigenenergies of H are distributed approximately in the energy interval $-6 < E_m < 10$. The main problem of this model is that its density of states is highly inhomogeneous with a strong peak in the middle of the energy band and this feature is not typical for a society with social stratification corresponding to an approximately constant density of states. To obtain a more realistic description of the model, we take into account the effect of social stratification by adding in (8) the diagonal matrix D with elements $D_{nn'} = D_n \delta_{nn'}$ where D_n is random and uniformly distributed in the interval $[-W/2, W/2]$. For $f = 0.1$, $W \geq 2$, the density of states $\nu(E_m) = dm/dE_m$ of the eigenenergies E_m of H is mainly determined by the diagonal elements D_n modeling social stratification of wealth in a society. In particular, $\nu(E_m) \approx N/B = \text{const}$ where the energy band width is roughly $B \approx W$. Both points are demonstrated in Fig. 1 for several values $2 \leq W \leq 16$.

We mention, that the results presented in Fig. 1 and other subsequent figures below concern one specific random realization of both matrices D and H^{GOE} in (8) but we verified that other random realizations give very close results. In particular, concerning H^{GOE} the coefficient $\kappa = 0.5$ is relatively weak producing essentially only a spectral smoothing of the eigenvalues of A .

It is convenient to characterize the eigenstates $\phi_n^{(m)}$ of the linear Hamiltonian H by the inverse participation ratio (IPR) $\xi = \left(\sum_n |\phi_n^{(m)}|^4 \right)^{-1}$ (assuming normalization $\sum_n |\phi_n^{(m)}|^2 = 1$) which is often used to describe the lo-

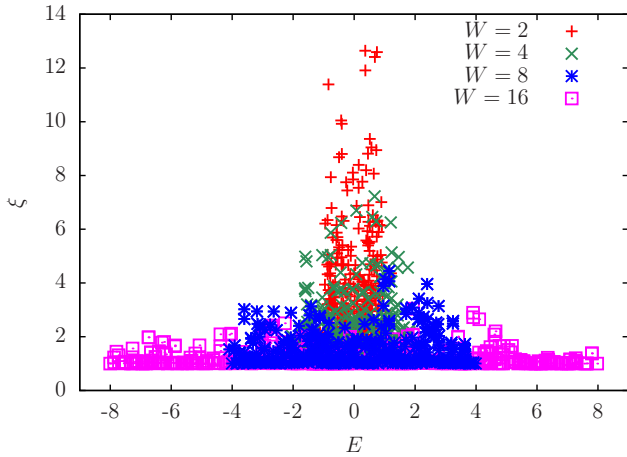


FIG. 2: Energy dependence of IPR ξ of eigenstates of the matrix H for the SSS model at $W = 2, 4, 8, 16$ given by (8) for $f = 0.1$ and $\kappa = 0.5$.

calization properties of eigenstates in disordered solids (see e.g. [43]) since the IPR ξ corresponds roughly to the number of nodes over which the eigenstate is localized. The dependence of the IPR on the eigenstate energy E is shown in Fig. 2. Typical values of ξ decrease with increasing parameter W since the factor f in (8) is relatively small. At the same time, the IPR seems to be randomly distributed with values in some interval $[1, \xi_{\max}]$ with the rough value $\xi_{\max} \sim 25/W$ and with smaller values at the spectral boundaries.

For comparison, the RMT model used in [20] corresponds to typical values $\xi \sim N$ where N is the size of the RMT-matrix with strongly ergodic eigenstates. Generally, we expect that for the issue of thermalization in (2), large ξ values are favorable to achieve thermalization more quickly and at more modest values of β (still slightly above the chaos border $\beta > \beta_{ch}$). Here for the SSS model typical values of ξ are much smaller. At $W = 8$, we have still many IPR values $\sim 2-3 > 1$ with some state mixing and also $W > f\bar{B} \approx 1.6$ where $\bar{B} \approx 16$ is the bandwidth of $A + \kappa H^{\text{GOE}}$. This value of W seems to be a reasonable compromise between significant mixing of states and dominant diagonal. Therefore, in the following, we fix $W = 8$, $\kappa = 0.5$, $f = 0.1$ in (8) which corresponds to a homogeneous stratification of energy and eigenstates. In our opinion, these parameters correspond to a typical social stratification in a society.

As illustration, we show in Fig. 3 the energy dependence of the temperature $T(E)$ and the chemical potential $\mu(E)$ for RJ thermalization obtained from the numerical solution of (5) together with the relation $T(E) = (E - \mu(E))/N$ for the eigenvalue spectrum of (8) for these parameters. Depending on $E < E_c$ ($E > E_c$), we have positive (negative) temperatures $T > 0$ ($T < 0$) and $\mu < E_1$ ($\mu > E_N$) where $E_c = (\sum_m E_m)/N$ is the center of mass for the energy spectrum. For our random realization of H we have $E_c = -0.053 \approx 0$. In Section III, we will present evidence for the presence of thermalization

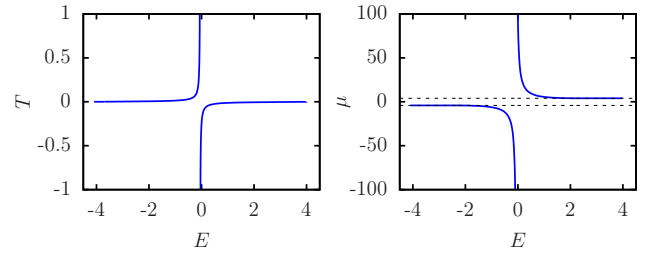


FIG. 3: The left (right) panel shows the temperature T (the chemical potential μ) versus energy E for the SSS model and the RJ case at $W = 8$, $f = 0.1$, $\kappa = 0.5$, $N = 379$. The dashed black lines in the right panel correspond to the values of $E_1 = -4.09$ and $E_N = 3.99$ (minimal and maximal energies E_m for the used random realization of H) showing that either $\mu < E_1$ (for $T > 0$) or $\mu > E_N$ (for $T < 0$). The transition from $T < 0$ to $T > 0$ happens at $E = E_c = -0.053$ for the given random realization of H used to compute the spectrum E_m .

of typical states at sufficiently large values of β (and the case $T > 0$).

In this work, we solve numerically the dynamical system (2) for the SSS model for the matrix H given by (8) using a symplectic 4th order integrator (see [20] and references therein). The advantage of this method is that it conserves exactly (up to usual numerical rounding errors) the quantity η while the energy \mathcal{H} is only approximately conserved. The numerical time integration step is chosen such that the numerical energy fluctuations of \mathcal{H} are well below 10^{-3} .

Usually, we start the time evolution (2) with an initial state $\psi(t = 0) = \phi_n^{(m_0)}$ located at the eigenmode with energy E_{m_0} , i.e. $C_m(t = 0) = \delta_{mm_0}$ ($= 1$ for $m = m_0$ and $= 0$ for $m \neq m_0$). Using the numerically obtained values of $C_m(t)$, we compute the mode probabilities ρ_m as the time average $\rho_m = \langle |C_m(t)|^2 \rangle$ over successive time intervals $2^{l-1} \leq t < 2^l$ for discrete integer values of $l = 1, 2, 3, \dots, l_{\max}$ with possible maximal values $l_{\max} = 30$ (i.e. $t_{\max} = 2^{30}$). These numerical ρ_m values, for a given time interval, can for example be used to compute numerical entropy values for both S_q and S_B which can be compared with their theoretical thermalized values (the results are presented in the next Section).

At exactly $t = 0$, we have formally $S_q = 0$ and $S_B \rightarrow -\infty$ since $\rho_m(t = 0) = |C_m(t = 0)|^2 = 0$ for $m \neq m_0$. However, due to the used time average procedure to compute ρ_m from $\langle |C_m(t)|^2 \rangle$ over successive intervals $2^{l-1} \leq t < 2^l$ the initial divergent value of S_B is not visible. In particular, the first used interval corresponds to $l = 1$ such that $1 \leq t < 2$ and the very initial time values $0 \leq t < 1$ are simply not used in our ρ_m data from which S_q and S_B are extracted by (7). Initial values $S_B(t = 2)$ obtained for the initial interval may be negative but typically they become rather quickly positive with increasing t , which is also due to our choice of the constant S_0 used in (7).

In this work, we consider the cases with nonlinear pa-

parameter $\beta \geq 2$ when the dynamics is clearly chaotic. We do not try to determine the precise value of the chaos border β_{ch} of this model since some discussion is given in [20]. Furthermore, the actual determination of the chaos border in a nonlinear system with many degrees of freedom is a complicated problem due to Arnold diffusion and other subtle nonlinear effects [10, 11].

C. Dissipative dynamics and turbulence in SSS

In [38] a particular modification of the dynamical system (2) (for the case of a random matrix $H = H^{\text{GOE}}$) was proposed to model Kolmogorov-Zakharov turbulence. The idea is to incorporate in the system norm and energy pumping at low energy scales and absorption at high energies. For a pumping strength above a certain chaos border, a global chaotic attractor appears with a stationary energy flow through the initial energy interval [13]. In this regime, the steady-state norm distribution is described by an algebraic decay with an exponent in agreement with the KZ theory. This distribution is close to the RJ one (3). Below the chaos border there is a KAM regime where the cascade flow is broken.

For the SSS model, as in [38], we rewrite Eq. (2) for the amplitudes $C_m(t)$ in the energy eigenbasis and add a new term for pumping and absorption [38]:

$$i \frac{\partial C_m}{\partial t} = E_m C_m + i(\gamma_m - \sigma_m |C_m|^2) C_m \quad (9)$$

$$+ \beta \sum_{m_1 m_2 m_3} V_{m m_1 m_2 m_3} C_{m_1} C_{m_2}^* C_{m_3} \quad ,$$

$$V_{m m_1 m_2 m_3} = \sum_n \phi_n^{(m)*} \phi_n^{(m_1)} \phi_n^{(m_2)*} \phi_n^{(m_3)} \quad . \quad (10)$$

For $\gamma_m = \sigma_m = 0$ (9) is exactly equivalent to (2) (taking into account the linear transformation $\psi_n \rightarrow C_m$). In (9) the transitions between linear eigenmodes appear only due to the nonlinear β -term with the transition matrix elements given by (10) in terms of the eigenmodes $\phi_n^{(m)}$. For the RMT case for H , as in [20, 38], they have typical values $V_{m m_1 m_2 m_3} \sim N^{-3/2}$ which are typically very small but all modes are coupled by them and there are many contributions of them in (9).

For the SSS model, corresponding to H given by (8), the situation is more complicated due to the reduced IPR values of the eigenmodes. If all four modes m, m_1, m_2, m_3 are roughly localized on the same nodes (of typical number $\sim \xi$), we have rather large (“maximal”) transition matrix elements $V_{m m_1 m_2 m_3} \sim \xi^{-3/2}$ but this value may be strongly reduced if the modes are localized on different nodes. Globally, this gives a very complicated dynamical system even for the Hamiltonian case $\gamma_m = \sigma_m = 0$.

Using non-zero values of $\gamma_m > 0$, $\sigma_m > 0$ in (9) we can model either pumping of modes or for $\gamma_m < 0$, $\sigma_m = 0$ dissipation of modes. In this case, the quantities η and \mathcal{H} are not conserved and the dynamical system (9) is no longer Hamiltonian. The positive value $\sigma_m > 0$ (if

$\gamma_m > 0$) implies that amplitudes of the corresponding modes typically saturate to $|C_m(t)| \rightarrow C_{\text{sat}} = \sqrt{\gamma_m / \sigma_m}$ at long times [38].

To model the energy flow of a direct cascade from low to high energy modes m we use pumping $\gamma_m = \gamma > 0$ for the 4 lowest energy modes at $m = 1, 2, 3, 4$ with corresponding saturation coefficients $\sigma_m = \sigma > 0$ and dissipation $\gamma_m = -\gamma < 0$, $\sigma_m = 0$ for the 4 highest energy modes with $m = N, N-1, N-2, N-3$. For all other m values we take $\gamma_m = \sigma_m = 0$. Here γ and σ are two parameters of the model and in most cases, as in [38], we choose $\gamma = \sigma = 0.01$ with saturation amplitude $C_{\text{sat}} = 1$ (for modes with $m \leq 4$).

For the case of an RMT matrix $H = H^{\text{GOE}}$, the properties of the KZ direct cascade have been discussed in detail in [38]. In this work here, we apply the same approach, based on Eq. (8) for H , to model the direct cascade of turbulent flow from low to high energies (or wealth values) in the SSS model. In a certain sense, this SSS turbulence system can be considered as a mathematical model of Marxist theory [1] when wealth is created by workers in the lowest wealth layer of society and it propagates to the layer with highest wealth being absorbed there.

As initial condition, we choose as in [38], random uniform values for the amplitudes $C_m(t=0)$ with $1 \leq m \leq 8$ such that the initial norm is $\eta(t=0) = 0.01$ and other initial amplitudes are $C_m(t=0) = 0$ (for $m > 8$). Furthermore, we use the same numerical method as in [38] which is an adapted version of the symplectic integrator used in [20]. We discuss the results and the properties of the steady-state distribution ρ_m in the SSS turbulence model in Section IV. Here, we mention briefly that the initial norm $\eta(t=0) = 0.01$ quickly increases and saturates at long times at values $\eta(t) \rightarrow \eta_{\text{sat}} \gg 1$. The numerical values ρ_m for the KZ case are obtained by the same time average $\rho_m = \langle |C_m(t)|^2 \rangle$ over intervals $t \in [2^{l-1}, 2^l]$, $l = 1, 2, \dots$. However, here $\eta = \sum_m \rho_m$ is no longer conserved.

III. RESULTS FOR HAMILTONIAN DYNAMICS OF THE SSS MODEL

In this Section, we present and discuss the numerical results for the Hamiltonian system of the SSS model obtained by solving (2) with the initial condition $\psi_n(t=0) = \phi_n^{(m_0)}$ (or equivalently $C_m(t=0) = \delta_{m m_0}$), i.e. the initial state is just the eigenmode $\phi^{(m_0)}$ of H . To obtain thermalization within numerically accessible time scales, we need to take a relatively strong nonlinear coefficient β since the relaxation rate to the steady-state is expected to be proportional to $\Gamma \propto \beta^2$ (as for the Fermi golden rule) such that the relaxation time behaves as $t_\Gamma \sim 1/\Gamma$. For this reason, we focus here on the two cases $\beta = 2$ and $\beta = 4$.

In order to establish the presence of RJ thermalization, we first compute from the numerical data both entropy

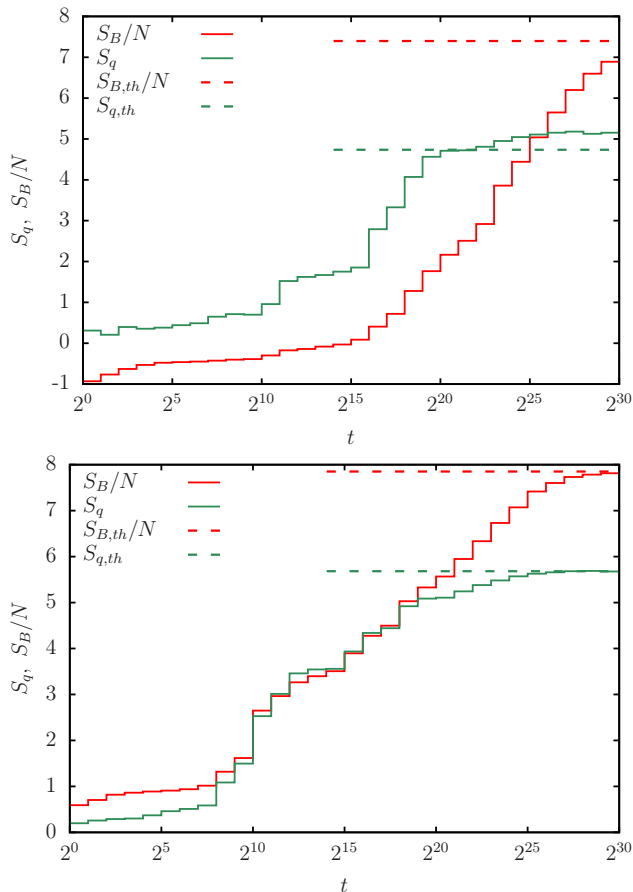


FIG. 4: Time dependence of von Neumann entropy $S_q(t)$ (full red line) and (rescaled) Boltzmann entropy S_B/N (full green line) for the SSS model; here $W = 8$, $N = 379$, $\beta = 2$ (top) and $\beta = 4$ (bottom); initial state is the linear eigenmode at $m_0 = 20$, i.e. $C_m(t=0) = \delta_{m,m_0}$. Entropy values are computed from (7) using time averaged $\rho_m = \langle |C_m(t)|^2 \rangle$ values for successive time intervals $2^{l-1} \leq t < 2^l$ for $l = 1, 2, 3, \dots, 30$. The dashed lines show the theoretical thermalized values, using (7) and the RJ values for ρ_m given by (3).

quantities given in (7). Their time dependence is shown in Fig. 4 for the initial mode $m_0 = 20$ and both values of β . Both entropy quantities increase with time and reach saturation at the theoretical values obtained from (7) using the theoretical RJ thermalized ρ_m values given in (3). It seems that at $\beta = 2$ the thermalization is not fully achieved at the largest time value $t = 2^{30}$ while for $\beta = 4$ the matching with the thermalized entropy values at the largest time is very good.

In Fig. 5, we show the energy dependence of the von Neumann entropy S_q . The blue curve corresponds to the theoretical thermalized energy dependence (obtained by combining (7) and (3)). The data points correspond to a selection of 23 states for different initial modes, including the 4 bottom ($m_0 = 1, 2, 3, 4$), the 4 top ($m_0 = N-3, N-2, N-1, N$) m_0 values and also the case $m_0 = 20$ (used in Fig. 4) for time values $2^{24} \leq t \leq 2^{27}$ (more precisely S_q is obtained from (7) with $\rho_m(t)$ being the average

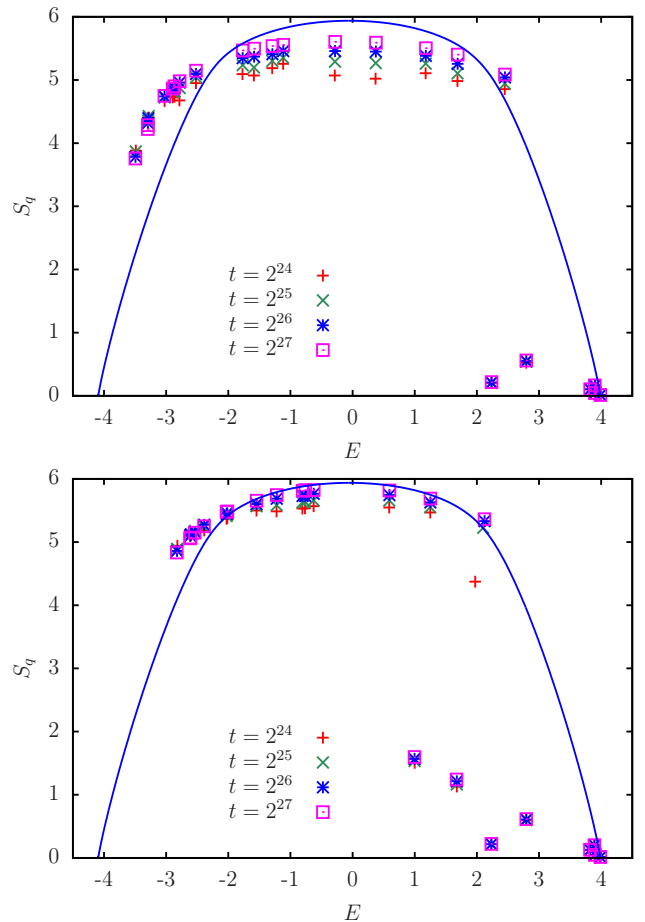


FIG. 5: Dependence of von Neumann entropy S_q on the average linear energy $E = \sum_m E_m \rho_m \approx \mathcal{H}$ for several initial eigenstates for different m_0 and t values for $\beta = 2$ (top) and $\beta = 4$ (bottom); the other parameters are $W = 8$, $f = 0.1$, $\kappa = 0.5$ and $N = 379$. The blue line shows the theoretical thermalized value of S_q . As in Fig. 4, S_q is computed from (7) using either numerically averaged ρ_m values (data points) or the thermalized RJ values (3) (blue line).

$\langle |C_m(\tau)|^2 \rangle$ for $\tau \in [t/2, t]$).

Before discussing the results shown in Fig. 5, we mention that for the data points the energy value E on the abscissa corresponds to the average linear system energy $E = \sum_m E_m \rho_m$ (Note that here and in the following we use the notation E only for the linear energy $E = \sum_m E_m \rho_m$). The value of the linear energy E may be quite different from the energy E_{m_0} of the initial mode due a significant energy shift effect caused by a quite large value of β and small initial IPR value ξ of the initial state. To see this more clearly, we write the global conserved energy \mathcal{H} of (1) at two time values $t = 0$ and $t = t_f$:

$$\mathcal{H} = E_{m_0} + \frac{\beta}{2\xi(t=0)} = \sum_n E_m \rho_m(t_f) + \frac{\beta}{2\xi(t_f)} \quad (11)$$

where $\xi(t)$ is the IPR of the state $\psi(t)$ at time t (in the initial node basis) and t_f is some long time value such

as $t_f = 2^{27}$ used in Fig. 5. At such times, and assuming thermalization, typical values of the IPR (of $\psi(t_f)$) are rather large $\xi(t_f) \gg 1$ such that the energy contribution of the non-linear term can be neglected and we have $\mathcal{H} \approx E = \sum_m E_m \rho_m(t_f)$. However, at $t = 0$, the initial state $\psi(t = 0)$, being the eigenmode $\phi^{(m_0)}$, has a rather small IPR value, typically below 3-4 (see Fig. 2), such that $\Delta E = \beta/(2\xi(t = 0)) \approx E - E_{m_0}$ takes significant values being around 10-20% of the bandwidth $B \approx 8$. For example, for $\beta = 4$ and $m_0 = 1$, we have $\xi(t = 0) = 1.52$, $E_1 = -4.09$, $E = \sum_m \rho(t_f)\rho(t_f) = -2.83$ with $\Delta E = 1.27$ which is close to $\beta/(2\xi(t = 0)) = 1.32$ (the remaining difference of 0.05 is due to the remaining small value of $\beta/(2\xi(t_f)) \ll 1$ in (11); residual technical fluctuations in the value of \mathcal{H} due to the numerical method are clearly below 10^{-3}).

This energy shift effect from $E_{m_0} \rightarrow E = E_{m_0} + \Delta E$ affects nearly all data points in Fig. 5. For $\beta = 2$ the linear energies are in the interval $-3.5 < E < 4$ and for $\beta = 4$ they are even in the interval $-3 < E < 4$ despite the fact that $E_1 = -4.09$ (which corresponds to the first data point with minimal E in both panels of Fig. 5). Since $\beta > 0$ this effect is favorable to achieve thermalization for modes with $E_{m_0} < 0$. For example for $m_0 = 1$ and $\beta = 4$ the initial linear energy is shifted from -4.09 to -2.83 and the latter provides a significant gap from the left spectral border which facilitates thermalization. The numerical values of S_q for $E < 0$ and a few data points at $E > 0$ shown in Fig. 5 approach with increasing time t indeed the theoretical RJ curve even though at $t = 2^{27}$ thermalization is not yet perfect, in particular for $\beta = 2$. Some modes with small m_0 value have actually values of S_q above the theoretical curve. In [20], it was also observed that S_q (for a mode with small m_0 value) is above the theoretical curve at intermediate time scales but at longer time scales it finally reaches the theoretical value (see SupMat Fig. S1 of [20]). We expect a similar behavior for the small m_0 modes in Fig. 5 where we have still S_q above the theoretical RJ curve for $t = 2^{27}$ but here the necessary time scales to reach the RJ curve are numerically not accessible.

However, for modes with $E_{m_0} > 0$ thermalization becomes more difficult due to the energy shift effect. There are two cases like this: the first one concerns the 4 top modes where $E_{m_0} \approx E_N = 3.98$. For these states it is impossible to have an energy shift effect since we have mathematically $E = \sum_m E_m \rho_m \leq E_N$ such that $\Delta E = E - E_{m_0} \approx 0$. Therefore, according to (11), the IPR $\xi(t_f)$ must be close to its initial value $\xi(t = 0)$ which is actually $\xi(t = 0) \approx 1$ for these 4 top modes (see also Fig. 2) and delocalization (thermalization) is simply impossible due to the conservation of \mathcal{H} . (Note that for negative $\beta < 0$ we would have such an effect at the lower spectral boundary.)

The second case of ‘‘difficult modes’’ concerns *some states* with small S_q values and with energies E above a certain threshold E_{th} (with $E_{th} \approx 2.2$ for $\beta = 2$ and $E_{th} \approx 1$ for $\beta = 4$) but still with a significant gap with

respect to the right spectral border $E_N = 3.98$. For these states, the S_q values also remain far from the RJ theory, clearly with $S_q > 0$ but also with $S_q < 0.6$ ($S_q < 2$) for $\beta = 2$ ($\beta = 4$). For such states, it is not impossible to have an energy shift effect. However, the data shows that for them we typically also have $E \approx E_{m_0}$ (at $t = 2^{27}$) resulting in a small IPR value and absence of thermalization. However, these states can still profit from the energy shift effect and it is indeed possible that thermalization for them sets in at much longer time scales than visible in Fig. 5 and numerically accessible.

There are also some (rather) well thermalized *other* modes with $E > E_{th}$ but closer inspection shows that for them we have $E_{m_0} < E_{th}$ and they have a strong energy shift effect (which allows the reduction of the IPR).

We also remind that the adjacency matrix A has significant degeneracies in its spectrum (see the detailed discussion in [35]) that still plays a role even when the GOE κ -term is added in (8). Furthermore, the matrix A is very sparse with a relatively small number of links per node $\chi \approx 4.82$ (for comparison other networks such as Wikipedia have $\chi \approx 20$). We think that both points are responsible for the observation that for the states with $S_q \approx 1-2$ (those with $E \approx E_{m_0} > E_{th}$) thermalization is very slow.

We note that similar type of deviations at high energies E have been seen in [35] without the stratification term D (see e.g. Fig.II.2 in [35]).

We do not show a figure for the energy dependence of S_B but the results are globally similar to Fig. 5 for S_q .

Examples of several probability distributions ρ_m obtained at large times are shown in Fig. 6 for $\beta = 2$ and Fig. 7 for $\beta = 4$ for the two initial modes $m_0 = 1, 20$. The results show that with an increase of total evolution time the values of ρ_m approach the theoretical RJ distribution (3). This process is more rapid for $\beta = 4$ than for $\beta = 2$ since the dynamical thermalization takes place only due to the nonlinearity with the relaxation rate $\Gamma \propto \beta^2$. The thermalization takes a long time to reach states at high energies but we expect that the thermalization will eventually reach these states at longer times. We note that a similar slow relaxation to the thermal state at high energies is also seen in the NLIRM model with diagonal matrix elements that approximately corresponds to the stratification term in the SSS model (see SupMat Fig. S14 in [20]).

We also note that in Figs. 6, 7 the RJ condensation fraction is relatively weak being e.g. about 25% of total norm in the linear groundstate eigenmode (see top panel in Fig. 6). This is essentially due to the energy shift effect. For example, for $m_0 = 1$ and $\beta = 4$, we have $E_{m_0} = E_1 = -4.09$ while for the RJ thermalization curve we need to use $E = \sum_m E_m \rho_m = -2.83$. In other systems the condensation fraction can be around 80-90% of total norm as e.g. for the NSE dynamics in quantum chaos fibers [23] or in the social networks without stratification term ($D = 0$ in (8)) [35].

Globally, the data presented in this Section strongly

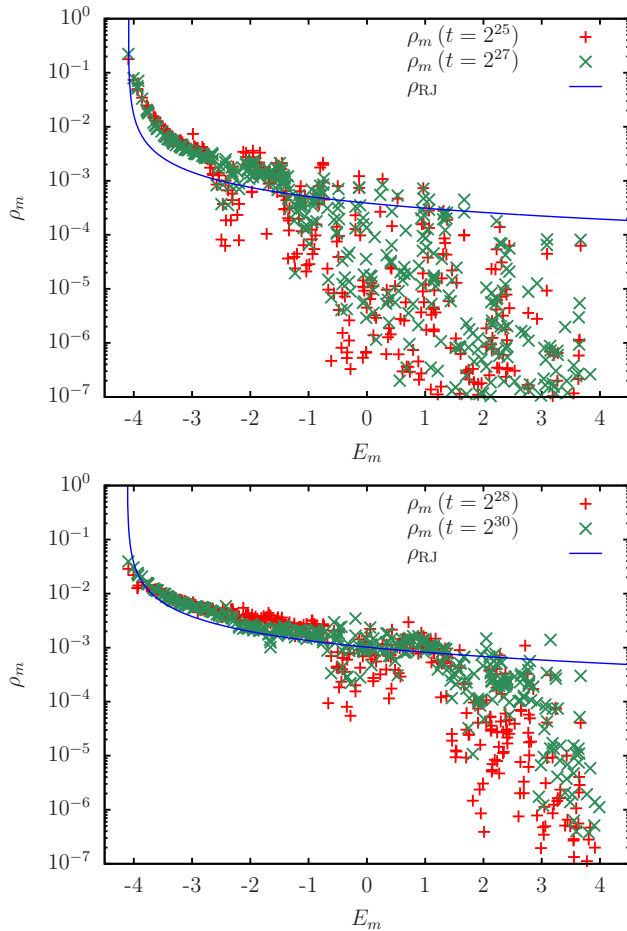


FIG. 6: Dependence of average eigenstate probability ρ_m on eigenstate energy E_m for the initial states at $m_0 = 1$ (top) and $m_0 = 20$ (bottom) at two different time values; the energy values are $E_{m_0} = -4.09$, $E = \sum_m E_m \rho_m = -3.49$ ($m_0 = 1$, top) and $E_{m_0} = -3.48$, $E = -2.52$ ($m_0 = 20$, bottom); the blue curve shows the theoretical RJ distribution (3) using the given value of E for each mode; other parameters are $\beta = 2$, $W = 8$, $f = 0.1$, $\kappa = 0.5$ and $N = 379$.

indicate the presence of RJ thermalization for the SSS model despite the sparse matrix structure of A and the strong diagonal with $W = 8$, which both tend to reduce typical IPR values of eigenstates. However, for this model it is more difficult to access the necessary numerical time scales and deviations for some modes with largest energies can be explained by the (absence of the) energy shift effect which is due to large β and small initial IPR values. Even though the adjacency matrix A has certain specific features (degeneracies, sparsity) we argue that it is important to use the data of a real social network of scientific collaboration [41] to study the properties of social stratification of society.

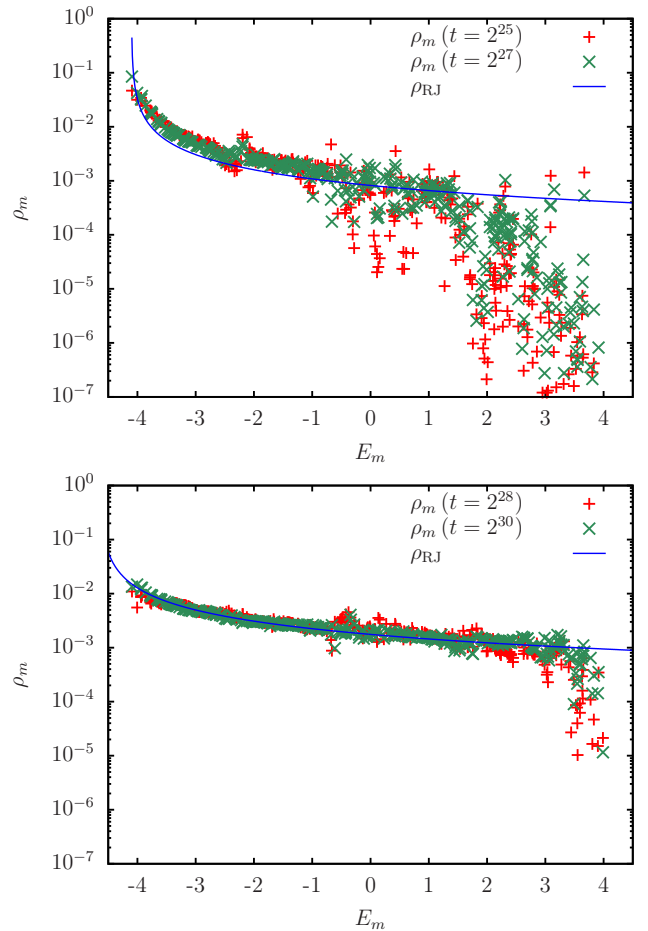


FIG. 7: Same as Fig. 5 but for $\beta = 4$ and energy values $E_{m_0} = -4.09$, $E = -2.83$ ($m_0 = 1$, top) and $E_{m_0} = -3.48$, $E = -1.55$ ($m_0 = 20$, bottom).

IV. RESULTS FOR KZ LIKE TURBULENCE IN SSS MODELS

In this Section we present results for the dynamical KZ turbulence in the SSS model described above in the Section II.C. In this model there is norm and energy pumping on the lowest $m = 1, 2, 3, 4$ states and absorption on highest states at $m = N - 3, N - 2, M - 1, N$. The initial condition at $t = 0$, corresponds to random uniform amplitudes $C_m(t = 0)$ for $1 \leq m \leq 8$ (and $C_m(t = 0) = 0$ for $m > 8$) with initial norm $\eta(t = 0) = \sum_m |C_m(t = 0)|^2 = 0.01$. A similar type of model of KZ turbulence (RMT of KZT) was studied in [38] for the case of an RMT matrix H .

The pumping leads to a growth of total norm η as it is shown in Fig. 8 for the SSS model (at $\beta = 4$, $N = 379$) and the RMT case taken from [38] (at $\beta = 1$, $N = 512$). After a certain time t_{st} a chaotic spreading of norm η over linear states reaches the states with absorption and the norm growth is stopped and the system enters in the steady-state regime. For both models, we have roughly $t_{st} \sim 2^{18}$. However, for the RMT model we have at

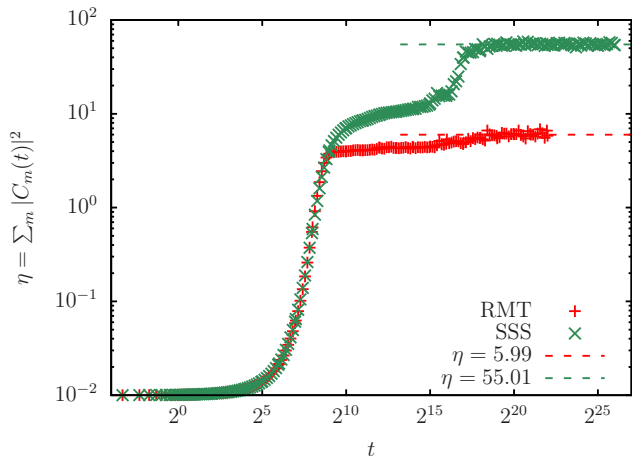


FIG. 8: Time dependence of the norm $\eta(t) = \sum_m |C_m(t)|^2$ (non-averaged) at selected time values for the SSS model ($\beta = 4$, $N = 379$) and RMT of KZT ($\beta = 1$, $N = 512$) from [38]. The norm values $\eta_{\text{av}} = \langle \eta(\tau) \rangle$ with average over the maximal time interval $t/2 \leq \tau \leq t$ are $\eta_{\text{av}} = 5.99$ (RMT of KZT, $t = 2^{22}$, $\beta = 1$) and $\eta_{\text{av}} = 55.01$ (SSS, $t = 2^{26}$, $\beta = 4$) (both indicated by dashed lines). Here $\gamma = \sigma = 0.01$ in the evolution of Eq. (9) with pumping, absorption, initial condition as described in Sec. II.C.

$t \sim 2^9$ an intermediate plateau only slightly below the final value while for the SSS model there is an additional increase of η for $2^{17} < t < 2^{19}$. We attribute this to the fact that the factor $f = 0.1$ in (8) is small and thus the linear links couple diagonal energy states in a relatively narrow energy band while for the RMT case in [38] such matrix transition couple all states inside the energy band.

In Fig. 9, we show the energy dependence of the steady-state norm distribution ρ_m obtained in the regime of KZ turbulence for the SSS model ($t = 2^{26}$) and the RMT model ($t = 2^{22}$). The time evolution of norm $\eta(t)$ for these two cases is shown in Fig. 8. At high energies both distributions demonstrate an approximate algebraic decay $\rho_m \propto 1/(E_m - E_g)^{s_0}$ with the exponents $s_0 = 1.130 \pm 0.004$ for the RMT case from [38] and $s_0 = 1.52 \pm 0.01$ for the SSS case. Here E_g is the approximate spectral lower boundary ($E_g = -4$ for SSS and $E_g = -1$ for RMT). For the RMT case the exponent s_0 is close to the theoretical value for the KZ turbulence [13, 38]. For the SSS model we have $s_0 = 1.52$ being noticeably higher than the theoretical value $s_0 = 1$. We attribute this deviation to a smaller system size (smaller N cases have higher s_0 values as it is seen for the RMT model cases in Fig. 1 of [20]). Also in the SSS model the links of the matrix A in (8) are rather local in energy, due to the small scaling factor $f = 0.1$ while in the RMT case and wave turbulence [13] the couplings have a significantly broader range. Fig. 9 shows results for $\gamma = 0.01$ for both models but we checked that for $\gamma = 0.005$ the results give rather similar algebraic like distributions ρ_m (apart from the total norm value).

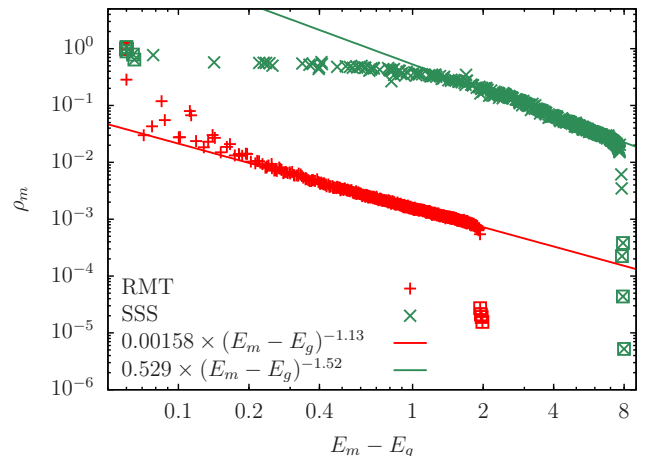


FIG. 9: Distribution ρ_m versus $E_m - E_g$ in a double logarithmic representation for the model of KZ turbulence of [38] with $\gamma = \sigma = 0.01$, pumping at $m = 1, \dots, 4$ and absorption at $m = N - 3, \dots, N$ (data points with boxed symbols); see text for the initial condition. Data points with $E_m - E_g < 0.06$ have been artificially moved to $E_m - E_g = 0.06$. The values of ρ_m have been obtained from the time average $\rho_m(t) = \langle |C_m(\tau)|^2 \rangle$ for $t/2 \leq \tau \leq t$. Red + symbols correspond to the RMT model of [38] for $N = 512$, $\beta = 1$, $t = 2^{22}$, $E_g = -1$ (same data as in Fig. 3 of [38]) and green \times symbols correspond to the SSS model introduced here for $N = 379$, $\beta = 4$, $t = 2^{26}$, $E_g = -4$. The straight lines show the power law fit $\rho_m = A(1 + E_m)^{-s_0}$ with $A = (1.584 \pm 0.003) \times 10^{-3}$, $s_0 = 1.130 \pm 0.004$, fit range $0.2 \leq E_m - E_g \leq 1.8$ (for RMT) and with $A = 0.5288 \pm 0.008$, $s_0 = 1.52 \pm 0.01$, fit range $1 \leq E_m - E_g \leq 7$ (for SSS). The values of the norm $\eta_{\text{av}} = \sum_m \rho_m$ are $\eta_{\text{av}} = 5.99$ (RMT) and $\eta = 55.01$ (SSS).

V. LORENZ CURVES FOR WEALTH INEQUALITY

In Sections I, II it is pointed out that the eigenenergies E_m of the linear Hamiltonian at $\beta = 0$ (8) can be also considered as individual wealth levels (layers or states) of a society with social stratification. In this framework, we can interpret the RJ thermal distribution (3) as wealth distribution for a population fraction $\rho_m = T/(w_m - \mu)$ over these wealth levels with $w_m = E_m - E_1$ (we apply a shift with E_1 to ensure that wealth levels are positive and have minimal value $w_1 = 0$). We remind that in this approach the thermal evolution of society wealth in the SSS model is produced by nonlinear interactions of society agents according to Eq. (2). This evolution has two integrals of motion being the total energy, or total wealth of society given by $w_s = \sum_m w_m \rho_m$, and the total norm of society population (or number of agents) $\eta = \sum_m \rho_m = 1$ normalized to unity. Indeed, the existence of two integrals of motion is rather natural since on a scale of one year there is only a relatively small variation of total wealth w_s and total norm η .

It is well known that the wealth distribution in the human society, e.g. in countries or the whole world, is

characterized by a striking inequality [36, 37, 44] and one may speculate in how far it is possible to attribute this inequality to the phenomenon of RJ condensation or more generally to the concentration of probability on low modes at low temperatures.

A wealth distribution is usually described by the Lorenz curve [44, 45] that gives the dependence of cumulated normalized wealth $w(h)$ on the cumulated normalized fraction of population or households h . Here, the hypothetical case of perfect equipartition of wealth corresponds to the diagonal $w(h) = h$ and the doubled area between diagonal and the Lorenz curve $w(h)$ determines the Gini coefficient $0 \leq G \leq 1$ [44, 46] that describes the overall degree of inequality. For the world countries the values of G can be found in [47] being in the range $0.59 < G < 0.90$ in 2021; for the whole world $G = 0.889$.

Let us assume that we have data for population fractions ρ_m with wealth levels w_m ($m = 1, \dots, N$, $0 = w_1 < w_2 < \dots < w_N$) where ρ_m may be obtained from the RJ distribution (of some “wealth” spectrum and given total energy/wealth) or from some other source (empirical data, numerically computed values of ρ_m for the models discussed in Sections II and III). Then we can construct the Lorenz curve as the set of points $(h(m), w(m))$ for $m = 0, 1, \dots, N$ with the partial sums $w(m) = \sum_{k=1}^m w_k \rho_k / w_s$ and $h(m) = \sum_{k=1}^m \rho_k$ such that $0 \leq h, w \leq 1$. Here the maximal value of h and w is $w(N) = h(N) = 1$ since $w_s = \sum_m w_m \rho_m$ and $\sum_m \rho_m = 1$.

In [35] a Wealth Thermalization Hypothesis (WTH) was introduced according to which the wealth shared in a country or the whole world is described by the Rayleigh-Jeans thermal distribution (3) using certain model spectra of w_m . This distribution depends on a dimensionless parameter $\varepsilon = w_s/B$ being the ratio of the total system wealth w_s on the its dispersion range $B = w_N$ determined by its highest value (or $\varepsilon = (E - E_1)/(E_N - E_1)$ if $E_1 \neq 0$ and with $w_s = E - E_1$). At relatively small values of ε there is the formation of an RJ condensate which leads to a huge fraction of poor households and a small oligarchic fraction which monopolizes a dominant fraction of total wealth thus generating a strong inequality in human society. It was shown that the WTH concept gives a good description of Lorenz curves for the wealth distributions in world countries and the whole world, stock exchange markets of New York, London, Hong Kong, Gross Domestic Product (GDP) of countries [35, 48].

In this work in the top panel of Fig. 10, we present several Lorenz curves for the RJ thermal distribution (3) with the (shifted) eigenvalue spectrum of the matrix H for the SSS model (8). Each curve corresponds to a given total energy of the system represented by the rescaled value $\varepsilon = w_s/B$ with $B \approx 8$. The Gini coefficient changes from $G = 0.33$ at $\varepsilon = 0.48$ to $G = 0.81$ at $\varepsilon = 0.1$ and $G = 0.96$ at $\varepsilon = 0.02$. At $\varepsilon = 0.1$ the fraction of poor households that owns 2% of total wealth is 67% while the oligarchic fraction of 10% richest households owns 63% of total wealth. Thus we see that the SSS model with RJ

condensate gives a good description of wealth inequality in the world countries described in [36, 37].

The bottom panel of Fig. 10 shows two Lorenz curves obtained from the numerical data for ρ_m of the states at $\beta = 4$, $m_0 = 1, 20$ (see also Fig. 7) using the (shifted) spectrum of the SSS model for the wealth levels. For comparison, we also present two Lorenz curves using RJ thermalized ρ_m values (as in top panel) for $\varepsilon = 0.32$ and $\varepsilon = 0.24$. The first value $\varepsilon = 0.32$ (with green Lorenz curve in both panels) corresponds indeed to $E = -1.55$ obtained from the numerical values ρ_m values by $E = \sum_m E_m \rho_m$ for the state with initial mode $m_0 = 20$ and it matches very well the direct numerical Lorenz curve (red data points in bottom panel of Fig. 10). This is not astonishing since for this state the numerical ρ_m values match indeed quite well the thermalized theoretical ρ_m values (see blue line and data points in bottom panel of Fig. 7).

We mention that for this state ($m_0 = 20$, corresponding to $\varepsilon = 0.32$) we have a Gini coefficient $G = 0.46$ and the fraction of poor households that owns 2% of total wealth is 18% while the oligarchic fraction of 10% richest households owns 27% of total wealth. This corresponds to a reduced inequality in comparison to the state at $\varepsilon = 0.1$ and real country/world data of [36, 37].

The other value $\varepsilon = 0.24$ (with blue Lorenz curve in both panels) has been obtained by matching the Gini coefficient of the numerical data for the state with $m_0 = 1$ (pink data points) with the RJ curve using the SSS model spectrum. However, here the linear energy $E = \sum_m E_m \rho_m = -2.83$ obtained from this state corresponds to $\varepsilon_{\text{num.}} = 0.16$ and its RJ Lorenz curve (only shown in top panel as pink curve) is significantly below the numerical Lorenz curve (for $m_0 = 1$). In top panel of Fig. 7, we indeed see that the RJ distribution of ρ_m (blue curve there) is somewhat shifted from the numerical data. The reason is that for this state many modes m with $E_m > 1.3$ have still ρ_m values clearly below the thermalized value and they give a significant reduction in the computation of $E = \sum_m E_m \rho_m$. However, these large energy modes, not yet thermalized, influence the numerical Lorenz curve only very slightly in the regime of very rich households (with $h \approx 1$). Therefore one can argue that for this state one can reduce the effective bandwidth $B = 8 \rightarrow (2/3)B = 5.33$ (of “well thermalized modes”) corresponding to a maximal cutoff energy $E_{\text{cut}} \approx 1.33$ in the top panel of Fig. 7. This reduction of B gives a rescaling $\varepsilon = 0.16 \rightarrow 0.16/(2/3) = 0.24$ which is indeed the value for the blue curve obtained by matching the Gini coefficient.

For this state ($m_0 = 1$, corresponding to $\varepsilon = 0.24$) we have a Gini coefficient $G = 0.55$ and the fraction of poor households that owns 2% of total wealth is 25% while the oligarchic fraction of 10% richest households owns 36% of total wealth. This corresponds to an “intermediate” inequality between the case $m_0 = 20$ ($\varepsilon = 0.32$) and $\varepsilon = 0.1$ and real country/world data of [36, 37].

We also compute Lorenz curves for the case of KZ tur-

bulence (see Section III and [38]). Here, we first remove first the 4 pumping modes ($m = 1, 2, 3, 4$) and the absorption modes ($m = N - 3, N - 2, N - 1, N$), we apply a shift using the new minimal value E_5 by $w_m = E_{m+4} - E_5$ for $1 \leq m \leq N - 8$ and then we normalize the remaining numerical ρ_m values (for $5 \leq m \leq N - 4$ with subsequent index shift $m + 4 \rightarrow m$ for $1 \leq m \leq N - 8$) to unity. Note that for the KZT case $\sum_m \rho_m \neq 1$ even after removing of pumping/absorption modes. Then we use the new shifted reduced spectrum and the renormalized ρ_m values to compute Lorenz curves as described above (including a recomputation of $w_s = \sum_m w_m \rho_m$).

We applied this procedure to the data of Fig. 9 for the RMT case of [38] ($\beta = 1, N = 512$) and the SSS model ($\beta = 4, N = 379$) for the steady state distribution of ρ_m in each case. The resulting Lorenz curves are shown Fig. 11. Here the fraction of poor households that owns 2% of total wealth is for the RMT (SSS) model 35% (16%) while the oligarchic fraction of 10% richest households owns 38% (32%) of total wealth.

We also compare the numerical Lorenz curves to the Rayleigh-Jeans standard (RJS) model (blue curves) introduced in [35] with values of ε determined by matching the Gini coefficients G to the numerical curves (obtained values of ε and G for both cases are given in the caption of Fig. 11) and the two blue curves for the RJS model match very nicely the numerical curves for the RMT and SSS models.

We remind that the RJS model corresponds to thermalized ρ_m values using a simple uniform spectrum $E_m = w_m = m/N$ which actually produces Lorenz curves very similar to the RJ Lorenz curves of the SSS model (shown in top panel of Fig. 10) since both have a (roughly) constant density of states for a shifted spectrum (i.e. with minimal wealth value $w_1 \approx 0$) and the different values of the bandwidth B do not affect the Lorenz curves (which are invariant to global energy rescaling). However, for Lorenz curves at small ε values (small T and large G) the effect of the first few levels is more strongly visible (case of RJ condensation) and therefore the precise structure of spacings between these first levels may generate some visible differences in the Lorenz curves between RJS and RJ for the SSS model.

We note that for KZ turbulence models the Lorenz curves are not very sensitive to the pumping rate γ as it is illustrated in Fig. 12 which compares the numerical curves of Fig. 11 obtained for $\gamma = 0.01$ to the case of $\gamma = 0.005$. However, the Lorenz curves are sensitive to the actual spectrum $w_m = E_m - E_1$ of shifted eigenenergies (or wealth levels of a society) as the difference between the RMT and SSS models show.

VI. DISCUSSION

In this work, we introduced a mathematical model of social stratification of society and studied its properties

with a nonlinear interactions between society members (or agents). In this SSS model the linear couplings between agents are described by an adjacency matrix of links represented by a real network of scientific collaboration taken from [41]. The social stratification, known to be present in a society [1–4], is described by an additional diagonal term of the linear Hamiltonian with eigenenergies E_m . These (shifted) E_m energies are interpreted as certain wealth levels w_m of society with $w_m = E_m - E_1$ counted from the ground state energy E_1 . The SSS model includes also nonlinear interactions of agents. The time evolution of the system is described by a nonlinear Hamiltonian with two integrals of motion being total system energy and total norm. Our studies show that above a certain chaos threshold of nonlinearity strength the nonlinear chaos leads to dynamical the RJ thermal distribution over linear eigenmodes with temperature and chemical potential determined by the values of two integrals. At low total energy this RJ distribution has a condensate phase that captures a significant fraction of total norm at low energy modes. This RJ condensation has been well studied theoretically and experimentally with mulimode optical fibers [23–30]. We also show that a model modification for energy and norm pumping at low energies and absorption at high energies in the SSS model demonstrates features of the KZ wave turbulence [13, 31, 32] with an algebraic probability distribution over system modes.

On the basis of the analogy between system mode energies and society wealth levels we show that the Lorenz curves obtained in the framework of the SSS model show close similarities with the wealth distribution in society [35–37, 48]. Thus we consider that the proposed mathematical SSS model provides a realistic thermodynamic description of wealth inequality in human societies.

Acknowledgments

This research has been partially supported through the grant NANOX N° ANR-17-EURE-0009 (project MTD-INA) in the frame of the *Programme des Investissements d’Avenir, France*. This work was granted access to the HPC resources of CALMIP (Toulouse) under the allocation 2026-P0110.

The data that supports the findings of this study are available within the article.

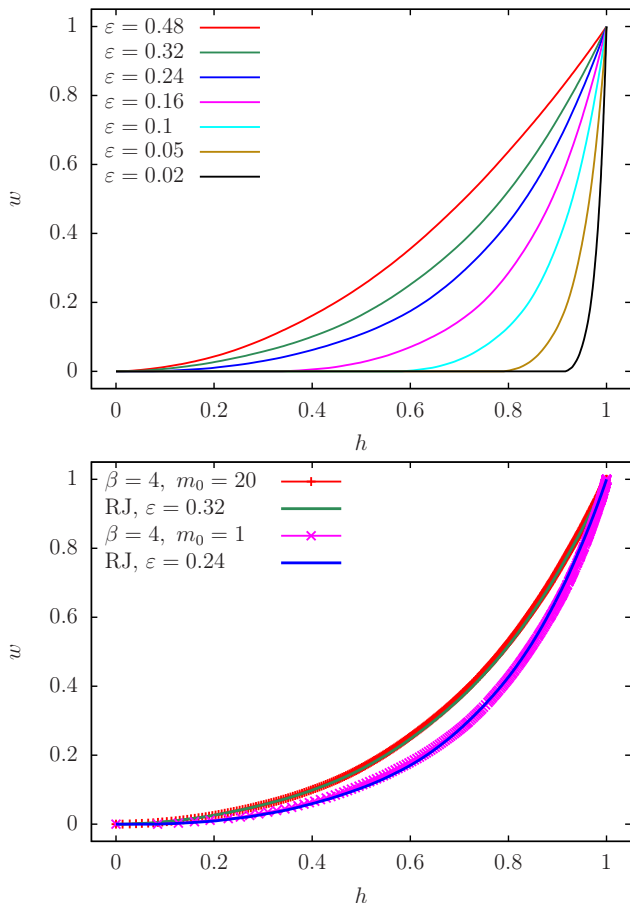


FIG. 10: *Top panel:* Lorenz curves using RJ thermalized ρ_m values for the spectrum of the SSS model at $W = 8$, $f = 0.1$, $\kappa = 0.5$, $N = 379$ for different rescaled total energies $\varepsilon = w_s/B$. The x -axis corresponds to the cumulated fraction of households (h) and the y -axis to the cumulated fraction of wealth (w). The Gini coefficients G for all curves are $G = 0.96, 0.9, 0.81, 0.71, 0.55, 0.46, 0.33$ (bottom to top). *Bottom panel:* Lorenz curves obtained from numerical ρ_m values of the states at $\beta = 4$ shown in Fig. 7 at maximal time $t = 2^{30}$ for the two initial modes $m_0 = 20$ (red + symbols) and $m_0 = 1$ (pink x symbols). The green (blue) curve corresponds to the Lorenz curve using RJ thermalized ρ_m values for the spectrum of the SSS model at $\varepsilon = 0.32$ ($\varepsilon = 0.24$). The ε value of the green curve corresponds to $\varepsilon = (E - E_1)/(E_N - E_1)$ where $E = \sum_m E_m \rho_m = -1.55$ is the average linear energy computed from the numerical ρ_m values of the state at $m_0 = 20$ and $t = 2^{30}$. The ε value of the blue curve has been obtained by matching the Gini coefficient between numerical data (at $m_0 = 1$) and the RJ curve. Both green and blue curves are identical to the curves of same color in the top panel with same ε values. Note that the numerical value $\varepsilon_{\text{num.}} = 0.16$ obtained from $E = -2.83$ for the state at $m_0 = 1$ is rather different to $\varepsilon = 0.24$ used for the blue curve and corresponds to the pink curve in top panel. The Gini coefficients for the numerical data are the same as in top panel for the green and blue curves.

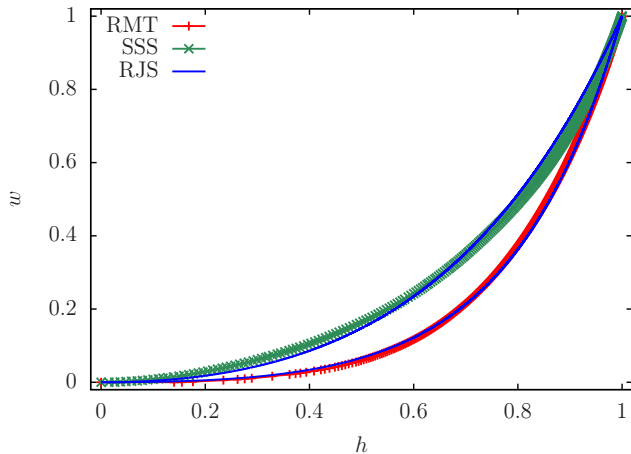


FIG. 11: Lorenz curves for dynamical turbulence for the two RMT and SSS models using the data of Fig. 9. The wealth and household variable w and h are computed as explained in the text using a shifted reduced spectrum without pumping/absorption modes and renormalized of remaining numerical ρ_m values taken from the data shown in Fig. 9. The full blue lines correspond to the Lorenz curves of the RJS model (using thermalized ρ_m values from a uniform spectrum of $N = 10000$ energies $E_m = m/N$) with the effective rescaled energy ε being determined to match the Gini coefficient G of the data (from RMT or SSS models): $\varepsilon = 0.202$, $G = 0.622$ (RMT) and $\varepsilon = 0.318$, $G = 0.48$ (SSS); $\gamma = \sigma = 0.01$ for both models.

-
- [1] K. Marx, *Das Kapital: Kritik der politischen Oekonomie. Vol. 1: Der Produktionsprozess des Kapitals (1 ed.)*, Verlag von Otto Meissner, Hamburg (1867); doi:10.3931/e-rara-25773
- [2] G.E. Lenski, *Power and privilege: A theory of social stratification*, Univ. North Carolina Press, Chapel Hill, USA (1984).
- [3] P. Sanders, *Social class and stratification* Routledge, London, UK (1990).
- [4] H.R. Kerbo, *Social Stratification and Inequality: Class Conflict in Historical, Comparative, and Global Perspective*, (9th ed.), Routledge, New York (2017).
- [5] Wikipedia, *Social stratification*, https://en.wikipedia.org/wiki/Social_stratification (Accessed on 23 February 2026).
- [6] S. Dorogovtsev, *Lectures in Complex Networks*, Oxford University Press, UK (2010).
- [7] M. Newman, *Networks*, Oxford University Press, UK (2018).
- [8] V. Arnold, A. Avez, *Ergodic problems of classical mechanics*, Benjamin, N.Y. (1968).
- [9] I. P. Cornfeld, S. V. Fomin and Ya. G. Sinai, *Ergodic theory*, Springer-Verlag, N.Y. (1982).
- [10] B. V. Chirikov, *A universal instability of many-dimensional oscillator systems*, Phys. Rep. **52**, 263 (1979).
- [11] A. Lichtenberg and M. Lieberman, *Regular and Chaotic Dynamics*, Springer, N.Y. (1992).
- [12] L.D. Landau, and E.M. Lifshitz, *Statistical physics*, Elsevier, Amsterdam (1980).
- [13] V.E. Zakharov, V.S. L'vov, and G. Falkovich, *Kolmogorov spectra of turbulence I*, Springer, Berlin, (1992).
- [14] E.Fermi, J.Pasta and S.Ulam, *Studies of non linear problems*, Los Alamos Report LA-1940 (1955); published later in E.Fermi *Collected papers*, E.Serge (Ed.) **2**, 491, Univ. Chicago Press, Chicago IL (1965); see also historical overview in T.Dauxois *Fermi, Pasta, Ulam and a mysterious lady*, Phys. Today **61(1)**, 55 (2008).
- [15] B.V. Chirikov and F.M. Izrailev, *Statistical properties of a non-linear string*, Sov. Phys. Doklady **11(1)**, 30 (1966).
- [16] B.V.Chirikov, F.M.Izrailev and V.A.Tayursky, *Numerical experiments on statistical behavior of dynamical systems with a few degrees of freedoms*, Comp. Comm. Phys. **5**, 11 (1973).
- [17] R. Livi, M. Pettini, S. Ruffo and A. Vulpiani, *Chaotic behavior in nonlinear Hamiltonian systems and equilibrium statistical mechanics*, J. Stat. Phys. **48**, 539 (1987).
- [18] G. Benettin, H. Christodoulidi and A. Poino, *The Fermi-Pasta-Ulam problem and its underlying integrable dynamics*, J. Stat. Phys. **152**, 195 (2013).
- [19] G.Gallavotti (Ed.), *The Fermi-Pasta-Ulam problem: a status report*, Lect. Notes Phys. **728**, Springer, Berlin (2008).
- [20] K.M. Frahm and D.L. Shepelyansky, *Nonlinear perturbation of Random Matrix Theory*, Phys. Rev. Lett. **131**, 077201 (2023).

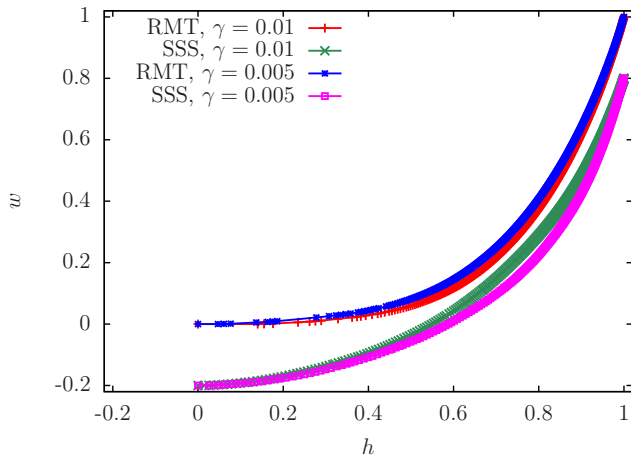


FIG. 12: Same as in Fig. 11, Lorenz curves are shown with numerical data of ρ_m for the SSS model and the RMT model of KZ from ([38]) for two values of strength pumping $\gamma = 0.01$ (as in Fig. 11) and $\gamma = 0.005$ ($\sigma = 0.01$ for all curves). The curves for SSS are artificially shifted down by 0.2 units in w for a better visibility. For $\gamma = 0.005$ we have $G = 0.585$, $\varepsilon = 0.235$ (RMT); $G = 0.533$, $\varepsilon = 0.227$ (SSS); for $\gamma = 0.01$ the related values are given in Fig. 11. Here the values of ε are determined from the RJS model by matching the Gini coefficients with the numerical data. The resulting RJS Lorenz curves are not shown but they match the numerical curves as in Fig. 11. For both models the Lorenz curves for the two γ values are rather close.

- [21] E.P. Wigner, *Random matrices in physics*, SIAM Review **9**(1), 1 (1967).
- [22] M.L. Mehta, *Random matrices*, Elsevier, Amsterdam (2004).
- [23] L. Ermann, A.D. Chepelianskii, and D.L. Shepelyansky, *Dynamical thermalization, Rayleigh-Jeans condensate, vortices and wave collapse in quantum chaos fibers and fluid of light*, J. Phys. A: Math. Theor. **59**, 055702 (2026).
- [24] A. Picozzi, J. Garnier, T. Hansson, P. Suret, S. Randoux, G. Millot and D.N. Christodoulides, *Optical wave turbulence: Towards a unified nonequilibrium thermodynamic formulation of statistical nonlinear optics*, Phys. Reports **542**, 1 (2014).
- [25] K. Krupa, A. Tonello, A. Barthelemy, B.M. Shalaby, A. Bendahmane, G. Millot and S. Wabnitz, *Observation of geometric parametric instability induced by the periodic spatial self-imaging of multimode waves*, Phys. Rev. Lett. **116**, 183901 (2016).
- [26] C. Connaughton, C. Josserand, A. Picozzi, Y. Pomeau, and S. Rica, *Condensation of classical nonlinear waves*, Phys. Rev. Lett. **95**, 263901 (2005).
- [27] K. Baudin, A. Fusaro, K. Krupa, J. Garnier, S. Rica, G. Millot, and A. Picozzi, *Classical Rayleigh-Jeans condensation of light waves: observation and thermodynamic characterization*, Phys. Rev. Lett. **125**, 244101 (2020).
- [28] E.V. Podivilov, F. Mangini, O.S. Sidelnikov, M. Ferraro, M. Gervaziev, D.S. Kharenko, M. Zitelli, M.P. Fedoruk, S.A. Babin, and S. Wabnitz, *Thermalization of orbital angular momentum beams in multimode optical fibers*, Phys. Rev. Lett. **128**, 243901 (2022).
- [29] H. Pourbeyram, P. Sidorenko, F.O. Wu, N. Bender, L. Wright, D.N. Christodoulides, and F. Wise, *Direct observations of thermalization to a Rayleigh-Jeans distribution in multimode optical fibres*, Nature Phys. **18**, 685 (2022).
- [30] K. Baudi, J. Garnier, A. Fusaro, N. Berti, C. Michel, K. Krupa, G. Millot, and A. Picozzi, *Observation of light thermalization to negative-temperature Rayleigh-Jeans equilibrium states in multimode optical fibers*, Phys. Rev. Lett. **130**, 063801 (2023).
- [31] S. Nazarenko, *Wave turbulence*, Springer-Verlag, Berlin (2011).
- [32] S. Galtier, *Physics of wave turbulence*, Cambridge Univ. Press, Cambridge UK (2023).
- [33] H. Fröhlich, *Bose condensation of strongly excited longitudinal electric modes*, Phys. Lett. A **26A**(9), 402 (1968).
- [34] H. Fröhlich, *Long-range coherence and energy storage in biological systems*, Int. J. Quantum Chemistry **II**, 641 (1968).
- [35] K.M. Frahm, and D.L. Shepelyansky, *Wealth thermalization hypothesis and social networks*, arXiv:2506.17720 [cond-mat.stat-mech] (2025).
- [36] T. Piketty, *Capital in the Twenty-First Century*, Belknap Press of Harvard University Press, Cambridge, MA (2014).
- [37] L. Chancel, T. Piketty, E. Saez, G. Zucman *et al.* *World Inequality Report 2022*, World Inequality Lab <https://wir2022.wid.world> (Accessed on 23 February 2026).
- [38] K.M. Frahm, and D.L. Shepelyansky, *Random matrix model of Kolmogorov-Zakharov turbulence*, Phys. Rev. E **109**, 044201 (2024).
- [39] M. E. J. Newman, *Network data*, <http://www.umich.edu/~mejn/netdata>, (Accessed 23 February 2025).
- [40] M. E. J. Newman, *Scientific collaboration networks. II. Shortest paths, weighted networks, and centrality*, Phys. Rev. E **64**, 016132 (2001).
- [41] M. E. J. Newman, *Finding community structure in networks using the eigenvectors of matrices*, Phys. Rev. E **74**, 036104 (2006).
- [42] M. E. J. Newman, *Community Centrality*, <http://www.umich.edu/~mejn/centrality> (Accessed 23 February 2026).
- [43] F. Evers, and A.D. Mirlin, *Anderson transitions*, Rev. Mod. Phys. **80**, 1355 (2008).
- [44] B. Roach, P. J. Rajkanikar, N. Goodwin, and J. Harris, *Social and Economic Inequality*, An ECI Teaching Module on Social and Environmental Issues, Economics in Context Initiative, Global Development Policy Center, Boston University (2023), <https://www.bu.edu/eci/files/2023/05/Inequality-Module-2023.pdf> (Accessed 23 February 2026).
- [45] M.O. Lorenz, *Methods of measuring the concentration of wealth*, Quarterly Publications of the American Statistical Association, **9**, (New Series, No. 70), 209–219 (1905); <https://doi.org/10.1080/15225437.1905.10503443> (Accessed 8 June 2025).
- [46] C. Gini, *Sulla misura della concentrazione e della variabilità a dei caratteri*, Atti del Reale Istituto Veneto di Scienze, Lettere ed Arti, **73**, 1203–1248 (1914); English translation in Metron - Int. J. Statistics, **63**, 3–38 (2005); <https://www.dss.uniroma1.it/RePec/mtn/articoli/2005-1-1.pdf> (Accessed 8 June 2025).
- [47] Wikipedia, *List of sovereign states by wealth inequality*, https://en.wikipedia.org/wiki/List_of_sovereign_

`states_by_wealth_inequality` (Accessed 23 February 2026).

- [48] K.M.Frahm and D.L.Shepelyansky, *Thermodynamic description of world GDP distribution over countries*, arXiv:2512.06420 [cond-mat.stat-mech] (2025).
- [49] For simplicity, we simply call the quantity η “norm” even though it actually corresponds to the “squared norm” $\|\psi\|^2 = \langle \psi | \psi \rangle = \sum_n |\psi_n|^2$ if $|\psi\rangle = \sum_n \psi_n |n\rangle$ is viewed

as a “quantum state” with time evolution (2) if $\beta = 0$.

[50] It is not difficult to verify that for a given spectrum E_m the transition from $T > 0$ to $T < 0$ happens at $E = E_c = (\sum_m E_m)/N$ where E_c is the “center of mass” of the energy spectrum. For the SSS model defined in Sec. II.B, we have $E_c \approx 0$.